Inorganic Chemistry
Article

Inorg. Chem. **2010**, *49*, 445–456 **445**
DOI: 10.1021/ic9013202

Crystal Growth, Transport, and the Structural and Magnetic Properties of Ln_4FeGa_{12} with Ln = Y, Tb, Dy, Ho, and Er

Brenton L. Drake,[†] Fernande Grandjean,*[,‡] Michael J. Kangas,[†] Edem K. Okudzeto,[†] Amar B. Karki,[§] Moulay T. Sougrati,[‡] David P. Young,[§] Gary J. Long,*[,∥] and Julia Y. Chan*[,†]

[†]*Department of Chemistry, Louisiana State University, 232 Choppin Hall, Baton Rouge, Louisiana 70803,* [‡]*Department of Physics, B5, University of Liège, B-4000 Sart-Tilman, Belgium,* [§]*Department of Physics and Astronomy, Louisiana State University, Baton Rouge, Louisiana 70803, and* [∥]*Department of Chemistry, Missouri University of Science and Technology, University of Missouri, Rolla, Missouri 65409-0010*

Received July 8, 2009

Ln_4FeGa_{12}, where Ln is Y, Tb, Dy, Ho, and Er, prepared by flux growth, crystallize with the cubic Y_4PdGa_{12} structure with the $Im\bar{3}m$ space group and with a = 8.5650(4), 8.5610(4), 8.5350(3), 8.5080(3), and 8.4760(3) Å, respectively. The crystal structure consists of an iron−gallium octahedra and face-sharing rare-earth cuboctahedra of the Au_3Cu type. $Er_4Fe_{0.67}Ga_{12}$ is iron-deficient, leading to a distortion of the octahedral and cuboctahedral environments due to the splitting of the Ga2 site into Ga2 and Ga3 sites. Further, interstitial octahedral sites that are unoccupied in Ln_4FeGa_{12} (Ln = Y, Tb, Dy, and Ho) are partially occupied by Fe2. Y_4FeGa_{12} exhibits weak itinerant ferromagnetism below 36 K. In contrast, Tb_4FeGa_{12}, Dy_4FeGa_{12}, Ho_4FeGa_{12}, and $Er_4Fe_{0.67}Ga_{12}$ order antiferromagnetically with maxima in the molar magnetic susceptibilities at 26, 18.5, 9, and 6 K. All of the compounds exhibit metallic electric resistivity, and their iron-57 Mössbauer spectra, obtained between 4.2 and 295 K, exhibit a single-line absorption with a 4.2 K isomer shift of ca. 0.50 mm/s, a shift that is characteristic of iron in an iron−gallium intermetallic compound. A small but significant broadening in the spectral absorption line width is observed for Y_4FeGa_{12} below 40 K and results from the small hyperfine field arising from its spin-polarized itinerant electrons.

Introduction

Several compounds in the Ln−M−Ga family, where Ln is a lanthanide and M is a transition metal, display strongly correlated electron behavior, such as magnetic ordering, superconductivity, heavy fermion behavior, and large magnetoresistance.[1] For example, several recently studied[2−4] compounds in the Ln−M−Ga family, where M is Ni, Pd, and Pt, exhibit large positive magnetoresistances of up to ca. 200% for La_2NiGa_{12} and Ce_2PdGa_{10}. Previously, we have grown single crystals of Ln_4MGa_{12}, where Ln is Tb, Dy, Ho, and Er and M is Pd and Pt.[5,6] The Pt analogues with Dy, Er, and Ho display a large positive magnetoresistance of 50, 220, and 900%, respectively.[6]

To study the role of magnetic transition metals in lanthanide−gallium compounds, we have explored several phases in the Ln−Fe−Ga system. This study has been motivated by the wide variety of thermal, electric, and magnetic properties of the iron-containing AFe_4Sb_{12} skutterudites,[7−10] where A, the so-called filling or rattling atom or ion, is an electropositive metal or ion. Depending on the nature of the electropositive metal, that is, the filling atom, in the filled skutterudites, the iron sublattice may or may not exhibit a magnetic moment. Whereas in most rare-earth and thallium-filled skutterudites[9,10] the iron atoms do

*To whom correspondence should be addressed. Tel.: (225) 578-2695. Fax: (225) 578-3458. E-mail: jchan@lsu.edu (J.Y.C.); glong@mst.edu (G.J. L.); fgrandjean@ulg.ac.be (F.G.).

(1) Thomas, E. L.; Millican, J. N.; Okudzeto, E. K.; Chan, J. Y. *Comments Inorg. Chem.* **2006**, *27*, 1–39.
(2) Cho, J. Y.; Millican, J. N.; Capan, C.; Sokolov, D. A.; Moldovan, M.; Karki, A. B.; Young, D. P.; Aronson, M. C.; Chan, J. Y. *Chem. Mater.* **2008**, *20*, 6116–6123.
(3) Millican, J. N.; Macaluso, R. T.; Young, D. P.; Moldovan, M.; Chan, J. Y. *J. Solid State Chem.* **2004**, *177*, 4695–4700.
(4) Williams, W. M.; Macaluso, R. T.; Moldovan, M.; Young, D. P.; Chan, J. Y. *Inorg. Chem.* **2003**, *42*, 7315–7318.
(5) Williams, W. M.; Moldovan, M.; Young, D. P.; Chan, J. Y. *J. Solid State Chem.* **2005**, *178*, 52–57.
(6) Cho, J. Y.; Moldovan, M.; Young, D. P.; Chan, J. Y. *J. Phys.: Condens. Matter* **2007**, *19*, 266224.
(7) Leithe-Jasper, A.; Schnelle, W.; Rosner, H.; Senthilkumaran, N.; Rabis, A.; Baenitz, M.; Gippius, A.; Morozova, E.; Mydosh, J. A.; Grin, Y. *Phys. Rev. Lett.* **2003**, *91*, 037208.
(8) Leithe-Jasper, A.; Schnelle, W.; Rosner, H.; Baenitz, M.; Rabis, A.; Gippius, A. A.; Morozova, E. N.; Borrmann, H.; Burkhardt, U.; Ramlau, R.; Schwarz, U.; Mydosh, J. A.; Grin, Y.; Ksenofontov, V.; Reiman, S. *Phys. Rev. B* **2004**, *70*, 214418.
(9) Viennois, R.; Ravot, D.; Terki, F.; Hernandez, C.; Charar, S.; Haen, P.; Paschen, S.; Steglich, F. *J. Magn. Magn. Mater.* **2004**, *272*, E113–E114.
(10) Leithe-Jasper, A.; Kaczorowski, D.; Rogl, P.; Bogner, J.; Reissner, M.; Steiner, W.; Wiesinger, G.; Godart, C. *Solid State Commun.* **1999**, *109*, 395–400.

Published on Web 12/18/2009

not carry any magnetic moment, in the filled $NaFe_4Sb_{12}$ and KFe_4Sb_{12} skutterudites, the iron sublattice displays ferromagnetic ordering with an effective magnetic moment of 1.6 μ_B per iron.[7,8] In contrast, $LaFe_4Sb_{12}$ exhibits paramagnetic behavior,[9] and the mixed valent Yb-filled $YbFe_4Sb_{12}$ skutterudite exhibits no magnetic moment on the iron sublattice, as is indicated by the magnetic and Mössbauer spectral measurements.[10]

With the goal of studying the effect of transition metals on the magnetization of the Ln_4MGa_{12} compounds, we have synthesized Ln_4FeGa_{12}, where Ln is Y, Tb, Dy, Ho, and Er. Herein, we report the crystal growth, structure, magnetic and transport measurements, and iron-57 Mössbauer spectral properties of these new Ln_4FeGa_{12} compounds.

Experimental Section

Synthesis. Single crystals of Ln_4FeGa_{12}, where Ln is Y, Tb, Dy, Ho, and Er, have been synthesized from their constituent elements by using Ln metals of at least 99.9% purity, Fe of 99.998% purity, and Ga of 99.99999% purity. All of the starting materials were obtained form Alfa Aesar and used as-received.

The elements were combined in a 1:1:20 molar ratio in an alumina crucible, covered with quartz wool, and sealed in an evacuated fused-silica tube. Each sample was then heated to 1423 K for 24 h and slowly cooled to 773 K at a rate of 15 K/h. Excess Ga flux was removed from the synthesized crystals by centrifugation, and when necessary, topical flux was removed by etching the recovered crystals in concentrated HCl. The $LnGa_6$ and Fe_3Ga_4 binary compounds were the dominant phases formed in the above synthesis, and the minor phase consisted of cubic crystals of Ln_4FeGa_{12}, crystals with a maximum dimension of 0.5 mm.

In order to determine whether the unexpected magnetic properties of Y_4FeGa_{12} were intrinsic or extrinsic, we varied the reaction profiles and conditions to optimize its synthesis; reaction profiles with reaction ratios of 2:1:20, 1:5:20, and 1:1:10 and with various dwell times were used. All of these reaction profiles resulted in YGa_6 and Fe_3Ga_4 as the dominant phases.

Arc melting of the constituent Y, Fe, and Ga elements in a 4:1:12 ratio resulted in a mixture of Y_4FeGa_{12} and YGa_6. In contrast, heating these elements in a 4:1:12 molar ratio in an induction furnace and subsequently annealing with a "seed crystal" of Y_4FeGa_{12} and excess Ga at 1423 K for 48 h, followed by slow cooling to 773 K at a rate of 5 K/h, resulted in a ca. 80% yield of the cubic Y_4FeGa_{12} phase. The seed crystal method was also used to synthesize single crystals of Tb_4FeGa_{12}, Dy_4FeGa_{12}, Ho_4FeGa_{12}, and $Er_4Fe_{0.67}Ga_{12}$, with yields of 90, 80, 70, and 60%, respectively. The cubic crystals obtained from the seed growth had a maximum volume of 9 mm^3; a picture of a crystal of Dy_4FeGa_{12} grown in a gallium flux is shown in Figure 1.

Polycrystalline samples of Tm_4FeGa_{12} were grown in an induction furnace, as described above. Unfortunately, the single crystals were not of sufficient quality to be suitable for structural analysis or physical property measurements. Finally, the yield was too small to allow accurate physical measurements. Attempts to grow single crystals of Yb_4FeGa_{12} resulted in the synthesis of the binary $YbGa_4$. Hence, this paper only reports results on the Ln_4FeGa_{12} compounds for which high-quality sizable crystals could be synthesized.

Multiple single crystals of Ln_4FeGa_{12} were selected for characterization by single-crystal X-ray diffraction and magnetization measurements. Further, several single crystals of Ln_4FeGa_{12} were ground and used for the Mössbauer spectral study. The homogeneity of the compounds was checked by powder X-ray diffraction.

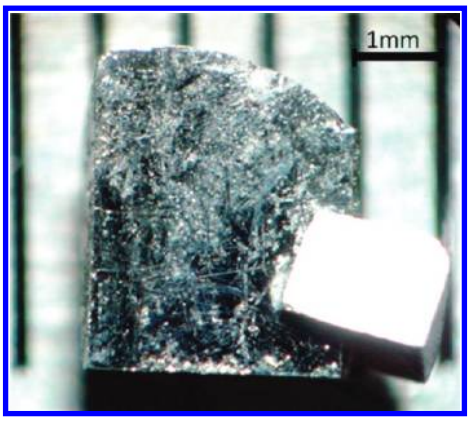

Figure 1. Photograph of crystals of Dy_4FeGa_{12}, silvery metallic, and grown with Ga flux, gray-black.

Single Crystal X-Ray Diffraction. Crystal fragments with dimensions of ca. 0.05 × 0.05 × 0.05 mm^3 were manually selected with an optical microscope for structural analysis. The crystals were glued onto a glass fiber and mounted on a Nonius Kappa CCD diffractometer that used 0.71073 Å Mo Kα radiation. Structural and refinement parameters are given in Table 1. The structure of Ln_4FeGa_{12}, where Ln is Y, Tb, Dy, Ho, and Er, was solved by direct methods using SHELXS97 and refined using SHELXL97;[11] the model of the refined structures were compared with that of the parent compound Y_4PdGa_{12}.[12] After refinement, the data were corrected for extinction effects and spherical absorption, and the displacement parameters were refined anisotropically. Table 2 gives the atomic positions and thermal displacement parameters for the above compounds. Additional information in CIF format is provided as Supporting Information.

Physical Measurements. Magnetic measurements on single crystals of Ln_4FeGa_{12} were performed by using the extraction magnetometer in a Quantum Design Physical Property Measurement System. The samples were held in place with Kapton tape. The magnetic susceptibilities have been measured after zero-field cooling to 2 K and subsequent warming to 310 K in an applied field of 0.1 T followed by field cooling from 310 to 2 K over a period of approximately 12 h. No significant difference was noted in the zero-field-cooled warming, and the field-cooled results and the two data sets have been merged to obtain the results presented herein. The magnetic susceptibilities, M/H, of the Ln_4FeGa_{12} compounds have been corrected for the diamagnetic contribution to the susceptibility by using Pascal's constants.

The magnetization of Y_4FeGa_{12} at 3, 10, 20, 30, 40, 50, 76, and 100 K and the magnetizations of the Ln_4FeGa_{12} compounds, where Ln is Tb, Dy, Ho, and Er, have been measured at 3 K in an applied field varying between 0 and 9 T.

The four-probe method has been used to measure the electrical resistivity of single crystals of Ln_4FeGa_{12} with a Quantum Design Physical Property Measurement System at ambient pressure. Platinum leads of 0.05 mm diameter were attached to the surface of the single crystals using silver epoxy, and resistivity measurements were obtained from 2 to 290 K.

The iron-57 Mössbauer spectra have been measured between 4.2 and 295 K in a Janis Supervaritemp cryostat with a constant-acceleration spectrometer which utilized a rhodium matrix cobalt-57 source and was calibrated at 295 K with α-iron powder. The Mössbauer spectral absorbers contained 26 mg/cm^2 of Y_4FeGa_{12} or 20 mg/cm^2 of Tb_4FeGa_{12}, Dy_4FeGa_{12}, or

(11) Sheldrick, G. M. In *SHELXL-97*; University of Göttingen: Göttingen, Germany, 1997.
(12) Vasilenko, L. O.; Noga, A. S.; Grin, Y. N.; Koterlin, M. D.; Yarmolyuk, Y. P. *Russ. Metall.* **1988**, 216–220.

Table 1. Unit Cell and Structural Refinement Parameters

compound	Y_4FeGa_{12}	Tb_4FeGa_{12}	Dy_4FeGa_{12}	Ho_4FeGa_{12}	$Er_4Fe_{0.67}Ga_{12}$
space group	$Im\bar{3}m$	$Im\bar{3}m$	$Im\bar{3}m$	$Im\bar{3}m$	$Im\bar{3}m$
a (Å)	8.5650(4)	8.5610(4)	8.5350(3)	8.5080(3)	8.4760(3)
V (Å^3)	628.32(5)	627.44(5)	621.74(4)	615.86(4)	608.94(4)
Z	2	2	2	2	2
cryst dimensions (mm^3)	0.05 × 0.05 × 0.5	0.05 × 0.05 × 0.05	0.05 × 0.05 × 0.05	0.05 × 0.05 × 0.05	0.03 × 0.03 × 0.04
temperature (K)	298(2)	298(2)	298(2)	298(2)	298(2)
ρ (g/cm^3)	6.597	8.089	8.239	8.370	8.417
θ range	3.36−29.86	3.37−29.88	3.38−29.98	3.39−29.85	2.55−34.97
μ (mm^{-1})	44.528	48.543	50.275	52.184	53.981
collected reflns	294	304	295	278	2130
unique reflns	103	108	105	107	159
h	$-11 \le h \le +12$	$-11 \le h \le +12$	$-11 \le h \le +12$	$-11 \le h \le +11$	$-13 \le h \le +13$
k	$-8 \le k \le +8$	$-8 \le k \le +8$	$-8 \le k \le +8$	$-8 \le k \le +8$	$-13 \le k \le +13$
l	$-7 \le l \le +7$	$-7 \le l \le +7$	$-7 \le l \le +7$	$-7 \le l \le +7$	$-13 \le l \le +12$
$\Delta\rho_{max}$ (e Å^{-3})	2.605	2.641	3.748	1.513	2.998
$\Delta\rho_{min}$ (e Å^{-3})	−1.631	−3.330	−2.342	−3.902	−4.102
R_1 (F)[a]	0.0382	0.0383	0.0305	0.0256	0.0304
R_w[b]	0.0655	0.0936	0.0871	0.0730	0.0500
GOF	1.165	1.298	1.238	1.230	1.161

[a] $R_1 = \sum||F_o| - |F_c||/\sum|F_o|$. [b] $R_w = [\sum[w(F_o^2 - F_c^2)^2]/\sum[w(F_o^2)^2]]^{1/2}$; $w = 1/[\sigma^2(F_o^2) + (0.00000P)^2 + 4.7941P]$, $w = 1/[\sigma^2(F_o^2) + (0.0390P)^2 + 7.8321P]$, $w = 1/[\sigma^2(F_o^2) + (0.0311P)^2 + 17.4653P]$, $w = 1/[\sigma^2(F_o^2) + (0.0138P)^2 + 20.5004P]$, and $w = 1/[\sigma^2(F_o^2) + (0.0000P)^2 + 39.2741P]$ for the Y, Tb, Dy, Ho, and Er compounds, respectively.

Er_4FeGa_{12} powder mixed with boron nitride. The quoted errors for the Mössbauer spectral parameters are the relative statistical errors; the absolute errors are approximately twice as large.

Results

Crystal Structures. The Ln_4FeGa_{12} compounds, where Ln is Y, Tb, Dy, Ho, and Er, all crystallize in the cubic Y_4PdGa_{12} structure, with the $Im\bar{3}m$, number 229, space group.[12,13] The crystal structure of Dy_4FeGa_{12}, as is shown in Figure 2a, consists of face-sharing $DyGa_3$ cuboctahedra with corner-sharing $FeGa_6$ octahedra. Selected bond distances are given in Table 3. The Fe−Ga2 interatomic distances are ca. 2.4 Å for all compounds, a distance that is only slightly smaller than the sum of the respective iron and gallium atomic radii of 1.24 and 1.22 to 1.25 Å, respectively.[13,14] The Ln−Ga_6 cuboctahedra in Ln_4FeGa_{12} have six Ln−Ga1 and six Ln−Ga2 interatomic distances of ca. 3.0 Å, see Table 3. These values are only slightly shorter than the sum of the atomic radii of the respective rare earth and gallium.

The structure of iron-deficient $Er_4Fe_{0.67}Ga_{12}$ is directly related to Dy_4FeGa_{12}, as can be seen in Figure 2b. Energy dispersive spectroscopy measurements yield an Er/Fe/Ga ratio of 4.2(2):0.53(5):11.8(3), a ratio that is in good agreement with the refined single crystal composition of $Er_4Fe_{0.67}Ga_{12}$. In $Er_4Fe_{0.67}Ga_{12}$, the unique Ga2 12*e* site, found in the other compounds, is divided into two crystallographically distinct sites, a Ga2 12*e* site and a second Ga3 12*e* site, each of which is half-occupied. This splitting results because of a partial 0.38(3) occupancy of the Fe1 site. As is shown in Figure 2b, when Fe1 is present, Ga2 is occupied and yields the expected octahedral coordination environment. If the Fe1 site is unoccupied, the Ga2 atoms move toward the octahedral hole, giving rise to occupancy of the Ga3 position and distorting the cuboctahedra such that it resembles the binary $ErGa_3$ ($Pm\bar{3}m$) subunit that is shown in Figure 2d. Inspection of the differences between the structures of $ErGa_3$ and $Er_4Fe_xGa_{12}$ indicates that $Er_4Fe_xGa_{12}$ is a body-centered variant of $ErGa_3$. Examination of the Fe1 local environment, as is

Table 2. Atomic Positions and Atomic Displacement Parameters

atom	Wyckoff site	x	y	z	U_{eq} (Å^2)[a]	occ.
			Y_4FeGa_{12}			
Y1	8*c*	1/4	1/4	1/4	0.0070(4)	1.0
Fe1	2*a*	0	0	0	0.0128(10)	1.0
Ga1	12*d*	1/4	0	1/2	0.0128(7)	1.0
Ga2	12*e*	0.2848(3)	0	0	0.0154(9)	1.0
			Tb_4FeGa_{12}			
Tb1	8*c*	1/4	1/4	1/4	0.0074(6)	1.0
Fe1	2*a*	0	0	0	0.0124(12)	1.0
Ga1	12*d*	1/4	0	1/2	0.0127(10)	1.0
Ga2	12*e*	0.2850(4)	0	0	0.0158(13)	1.0
			Dy_4FeGa_{12}			
Dy1	8*c*	1/4	1/4	1/4	0.0051(5)	1.0
Fe1	2*a*	0	0	0	0.0148(15)	1.0
Ga1	12*d*	1/4	0	1/2	0.0109(10)	1.0
Ga2	12*e*	0.2828(4)	0	0	0.0184(13)	1.0
			Ho_4FeGa_{12}			
Ho1	8*c*	1/4	1/4	1/4	0.0082(5)	1.0
Fe1	2*a*	0	0	0	0.0208(14)	1.0
Ga1	12*d*	1/4	0	1/2	0.0128(9)	1.0
Ga2	12*e*	0.2814(4)	0	0	0.0237(12)	1.0
			$Er_4Fe_{0.67}Ga_{12}$			
Er1	8*c*	1/4	1/4	1/4	0.0080(2)	1.0
Fe1	2*a*	0	0	0	0.007(4)	0.38(3)
Fe2	6*b*	1/2	0	0	0.010(9)	0.096(16)
Ga1	12*d*	1/4	0	1/2	0.0144(4)	1.0
Ga2	12*e*	0.280(4)	0	0	0.017(4)	0.5
Ga3	12*e*	0.249(4)	0	0	0.017(4)	0.5

[a] U_{eq} is defined as one-third of the trace of the orthogonalized U_{ij} tensor.

(13) Zhuravleva, M. A.; Wang, X. P.; Schultz, A. J.; Bakas, T.; Kanatzidis, M. G. *Inorg. Chem.* **2002**, *41*, 6056–6061.

(14) (a) Emsley, J. *The Elements*; Oxford University Press: New York, 1999; p 1. (b) Sutton, L. *Tables of Interatomic Distances and Configurations in Molecules and Ions, Vol. Spec. Publ. No. 18*; The Chemical Society: London, 1965.

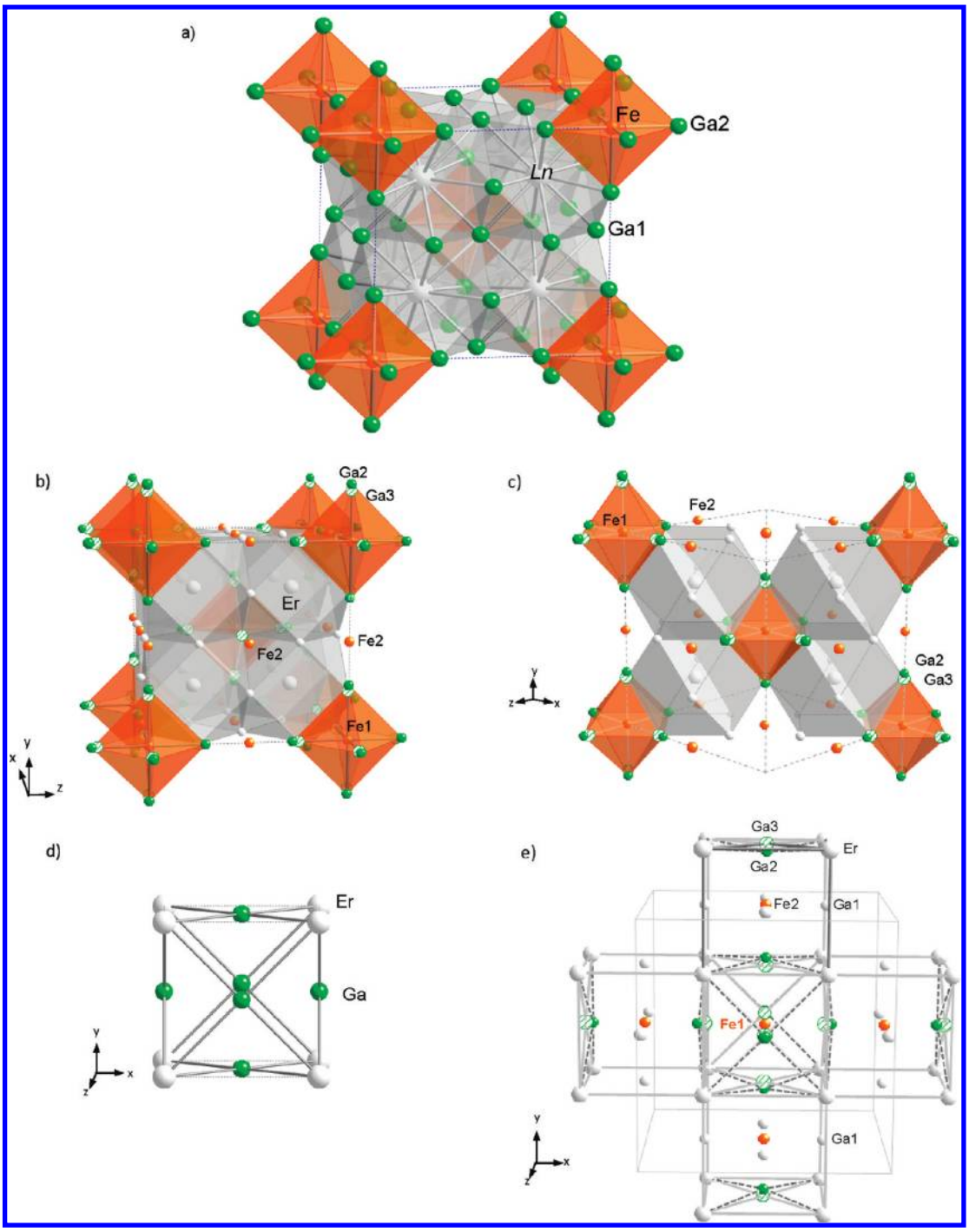

Figure 2. (a) The crystal structure of Dy_4FeGa_{12}. The Dy, Fe, and Ga atoms are shown in gray, orange, and green, respectively. (b) The crystal structure of $Er_4Fe_{0.67}Ga_{12}$. Er and Ga1 are shown in gray; Fe1 and Fe2 are shown in orange, and Ga2 and Ga3 are shown in solid green and green striped spheres, respectively. (c) The local erbium and iron environments along the [101] plane. (d) Primitive unit cell of $ErGa_3$ ($Pm\bar{3}m$). (e) Simple cubic packing $ErGa_3$ subunits with iron partially occupying the interstitial sites to form $Er_4Fe_{0.67}Ga_{12}$.

shown in Figure 2e, indicates that the presence of Fe1 yields the isostructural environment of Dy_4FeGa_{12}. If Fe1 is unoccupied, the structure collapses to that of $ErGa_3$. The $Er_4Fe_{0.67}Ga_{12}$ compound is the end member of the Ln_4FeGa_{12} series, and the Tm and Yb analogues cannot be stabilized based on our synthetic methods. This observation is consistent with the partial occupancy found in the Er phase. This inability is observed in $Er_4Fe_{0.67}Ga_{12}$ as the partial occupancy of the Fe1 position. With Tm_4FeGa_{12}, the body-centered Fe1 position is not favored, and thus, the 1:3 primitive binary compound is formed. As may also be seen in Figure 2b and c, an Fe2 site with a 0.096(16) occupancy is observed and occupies the octahedral holes unoccupied by Fe1. A close inspection of the Fe2 environment once again reveals a remarkable resemblance to the 1:3 binary structure. The best description of the structure of $Er_4Fe_xGa_{12}$ is that of an intergrowth of the $ErGa_3$ and Er_4FeGa_{12} structures. Thus, the structure of $Er_4Fe_xGa_{12}$ can be viewed as a primitive cubic packing of $ErGa_3$ with half of the cubes

Table 3. Selected Intermetallic Distances

	Y_4FeGa_{12}	Tb_4FeGa_{12}	Dy_4FeGa_{12}	Ho_4FeGa_{12}	$Er_4Fe_{0.67}Ga_{12}$
			Ln Cuboctahedra		
Ln1−Ga1 (×6)	3.02818(14)	3.02677(14)	3.01758(11)	3.00803(11)	2.99672(11)
Ln1−Ga2 (×6)	3.0428(3)	3.0416(4)	3.0305(4)	3.0199(4)	3.008(3)
Ln1−Ga3 (×6)[a]					2.99673(14)
Ga1−Ga2 (×4)	2.825(1)	2.823(2)	2.827(2)	2.825(2)	2.82(2)
			Fe Octahedra		
Fe1−Ga2 (×6)	2.439(2)	2.440(4)	2.413(4)	2.394 (4)	2.37(4)

[a]Ga3 is only present when Fe1 does not occupy the center of the octahedral hole.

occupied by Fe1 and Fe2. In this view, Fe1 and Fe2 are crystallographically equivalent because they both occupy the 1/2, 1/2, 1/2 position of the primitive unit cell of $ErGa_3$. This description effectively reproduces the $Er_4Fe_xGa_{12}$ structure when x is sufficiently high, such that the full symmetry of the body-centered cubic structure is observed by single-crystal diffraction.

The dependence of the Ln−Ga1, Ln−Ga2, Fe−Ga2, and Ga1−Ga2 distances upon the rare-earth atomic number is shown in Figure S1 in the Supporting Information. The first three distances decrease with increasing rare-earth atomic number, as a result of the lanthanide contraction, whereas the Ga1−Ga2 distance remains constant.

Magnetic Properties of Y_4FeGa_{12}. The temperature dependence of the molar magnetic susceptibility of Y_4FeGa_{12}, measured in an applied dc field of 0.1 T, is shown in Figure 3a, and the analogous $\chi_M T$ plot is shown in the inset to this figure. At first, one might think that the single iron in Y_4FeGa_{12} is undergoing long-range magnetic ordering below ca. 36 K. But this is not the case, as is indicated by the rapid decrease in $\chi_M T$ below 18 K, by the very small magnitude of the molar magnetic susceptibility below 36 K, by the large minimum Fe−Fe separation of 7.4175(4) Å along the body-diagonal of the unit cell, and by the Mössbauer spectra, to be discussed below. A similar temperature dependence of the magnetic susceptibility was observed in $Fe_{2.5}Co_{0.5}Mo_3N$ by Pryor and Battle[15] and assigned to an atomic disorder that induces a spin-glass behavior; an assignment that does not apply to the perfectly ordered Y_4FeGa_{12} structure. The magnetization curve of Y_4FeGa_{12}, measured at 3 K in an applied dc field of up to 9 T, is shown in Figure 3b. The magnetization increases sharply in an applied field of 0.005 T and reaches 0.14 μ_B per formula unit of Y_4FeGa_{12} and increases further, almost linearly, to 0.22 μ_B at 9 T without reaching saturation; there is no hysteresis around a zero-applied field.

The temperature dependence of the inverse magnetic susceptibility of Y_4FeGa_{12} exhibits a negative curvature at high temperatures and does not show any clear linear behavior over a wide temperature range, even at high temperatures, see Figure S2 in the Supporting Information. A Curie−Weiss fit of the inverse susceptibility between 45 and 70 K gives an effective magnetic moment, μ_{eff}, of 1.55 μ_B per mole of Fe and a Weiss temperature of 34 K, a positive temperature that suggests a ferromagnetic behavior.

Several of the magnetic properties of Y_4FeGa_{12} described above suggest that Y_4FeGa_{12} is a very weak itinerant ferromagnet. In a fashion similar to some yttrium−cobalt intermetallics,[16,17] such as Y_4Co_3 and

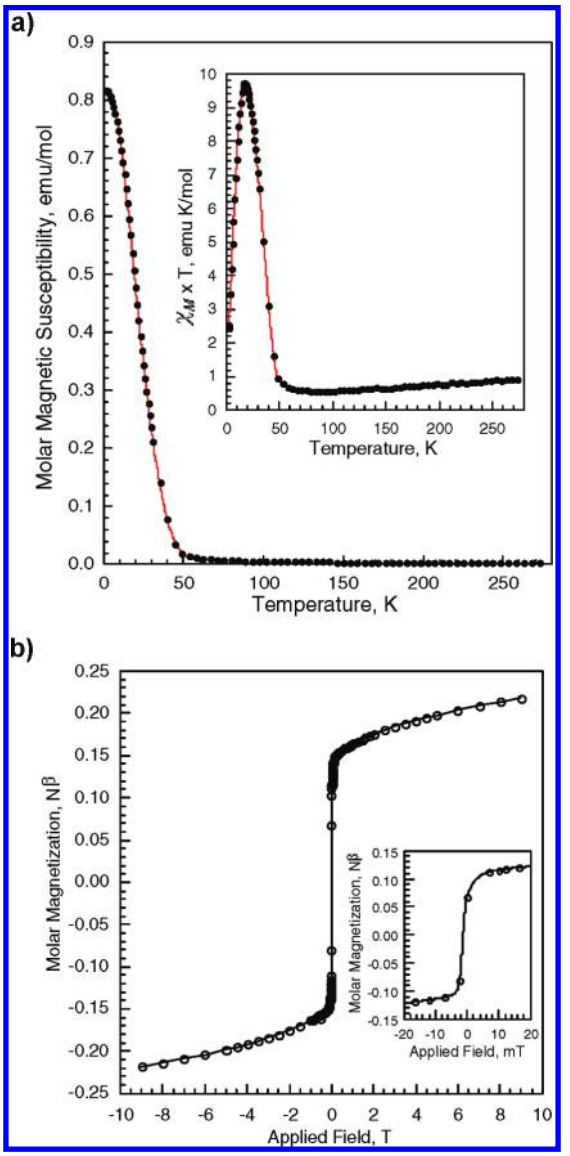

Figure 3. (a) The temperature dependence of the molar magnetic susceptibility of Y_4FeGa_{12} measured in a 0.1 T dc applied field. Inset: The temperature dependence of $\chi_M \times T$. (b) The magnetization of Y_4FeGa_{12} measured at 3 K as a function of dc applied magnetic field. Inset: An enlargement about zero applied field.

(15) Pryor, T. J.; Battle, P. D. *J. Mater. Chem.* **2004**, *14*, 3001.

(16) Kolodziejczyk, A.; Spalek, J. *J. Phys. F* **1984**, *14*, 1277.
(17) Yamaguchi, Y.; Nishihara, Y.; Ogawa, S. *J. Phys. Soc. Jpn.* **1984**, *53*, 3985.

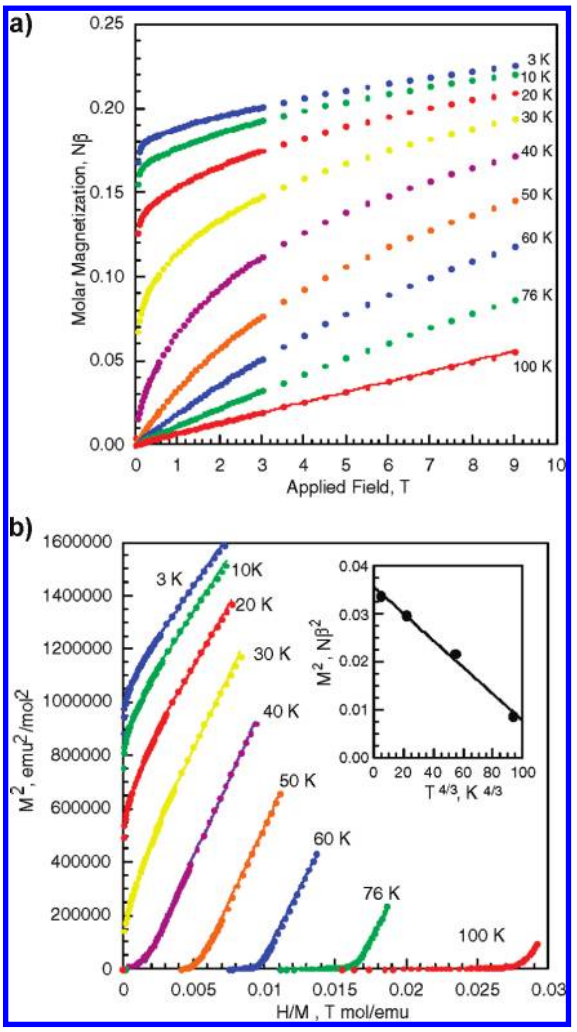

Figure 4. (a) The magnetization of Y_4FeGa_{12} obtained at the indicated temperatures. (b) The Arrott plots for Y_4FeGa_{12}. Inset: The square of the magnetization extrapolated to zero applied field at 3, 10, 20, and 30 K as a function of $T^{4/3}$.

Y_9Co_7, its very small magnetization does not saturate in a field of 9 T, see Figure 3b, its μ_{eff} obtained between 45 and 70 K is larger than its 3 K moment under a small applied field, and its inverse magnetic susceptibility shows a negative curvature at high temperature, see Figure S2 (Supporting Information); these three observations are characteristic signatures of an itinerant ferromagnet.

In order to evaluate this model, the magnetization of Y_4FeGa_{12} has been measured at 3, 10, 20, 30, 40, 50, 60, 76, and 100 K in an applied field between 0 and 9 T; the field dependence of the magnetization is shown in Figure 4a. At 76 and 100 K, Y_4FeGa_{12} exhibits paramagnetic behavior, whereas between 3 and 60 K, the magnetization does not saturate even at 9 T. The Arrott plots, that is, the square of the magnetization versus the applied field divided by the magnetization, for Y_4FeGa_{12} are shown in Figure 4b. As expected[16,17] for an itinerant ferromagnet, over a rather large range of applied fields, these curves can be fit with straight lines. Clearly, the shape of these curves changes between 30 and 40 K, indicating that the itinerant electron ferromagnetic ordering temperature is between 30 and 40 K. The magnetization extrapolated to zero field at 3, 10, 20, and 30 K, as obtained from the linear fits shown in Figure 4b, is plotted as its square versus $T^{4/3}$ in the inset to Figure 4b. Spin fluctuation theory[18] for itinerant ferromagnetism predicts a linear behavior for this plot, as is observed.

The Rhodes−Wohlfart parameter, P_C/P_S, where P_C is the paramagnetic moment and P_S is the zero-temperature zero-field magnetic moment, should be greater than one for an itinerant ferromagnet. The P_C may be estimated two different ways. First, from the Curie−Weiss fit of the inverse susceptibility described above, $P_C = 0.84\ \mu_B$ is obtained from $\mu_{eff} = 1.55\ \mu_B = [P_C(P_C + 2)]^{1/2}$. Second, because in an itinerant ferromagnet there is a temperature-independent contribution to the magnetic susceptibility, χ_0, the Pauli paramagnetic susceptibility, the magnetic susceptibility of Y_4FeGa_{12} was fitted with the so-called modified Curie−Weiss law, $\chi = \chi_0 + C/(T - \theta)$, where C is the Curie constant and θ is the Weiss temperature. χ_0, C, and θ refine to 0.0026 emu/mol, 0.20 emuK/mol, and 37.2 K, respectively. The Pauli paramagnetic susceptibility, χ_0, is slightly larger than the value of 0.00194 emu/mol reported[17] for Y_9Co_7. From the Curie constant, $P_C = 0.61\ \mu_B$ is obtained from $\mu_{eff} = 1.26\ \mu_B = [P_C(P_C + 2)]^{1/2}$.

P_S may be estimated to be 0.18 μ_B from the 3 K magnetization linear fit in Figure 4b extrapolated to zero field. Thus, for Y_4FeGa_{12}, the Rhodes−Wohlfart parameter, P_C/P_S, is between 4.67 and 3.40 if the first or the second method for the determination of P_C is used. These values are greater than one and strongly indicate that Y_4FeGa_{12} is a weak itinerant ferromagnet. For comparison, Y_4Co_3 and Y_9Co_7 have Rhodes−Wohlfart parameters[16,17] of 11.5 and 9.6.

Because Y_4FeGa_{12} shows a nonzero magnetization below 30 K, the Stoner criterion for ferromagnetism appears to be satisfied. However, if it was not satisfied, the Pauli paramagnetic susceptibility of Y_4FeGa_{12} would be multiplied by the Stoner enhancement factor,[16] $\alpha = 1 + (2/27)P_S^2$, that is equal to 1.0024, an enhancement that may lead to the slightly large value of χ_0.

Electrical Properties of Y_4FeGa_{12}. The temperature dependence of the resistivity of Y_4FeGa_{12} is analyzed[16,19] in Figure 5 in the framework of the spin fluctuation theory, a theory that predicts that, below the magnetic ordering temperature, the temperature dependence of the resistivity follows the square of the temperature. The inset in Figure 5 shows that, below 30 K, the temperature dependence of the resistivity is well-fitted with a quadratic dependence of the temperature. Between 30 and 100 K, the resistivity increases linearly with temperature, and above 100 K it increases as $T^{0.43}$. A similar temperature dependence of the resistivity has been reported[16] for Y_4Co_3.

In conclusion, Y_4FeGa_{12} shows the characteristic magnetic and electric behavior of a weak itinerant ferromagnet. In these cases, the magnetic moments are not localized on the iron but are delocalized and carried by the conduction electrons.

(18) Makoshi, K.; Moriya, T. *J. Phys. Soc. Jpn.* **1975**, *38*, 10.
(19) Ueda, K.; Moriya, T. *J. Phys. Soc. Jpn.* **1975**, *39*, 605. Ueda, K. *Solid State Commun.* **1976**, *19*, 965.

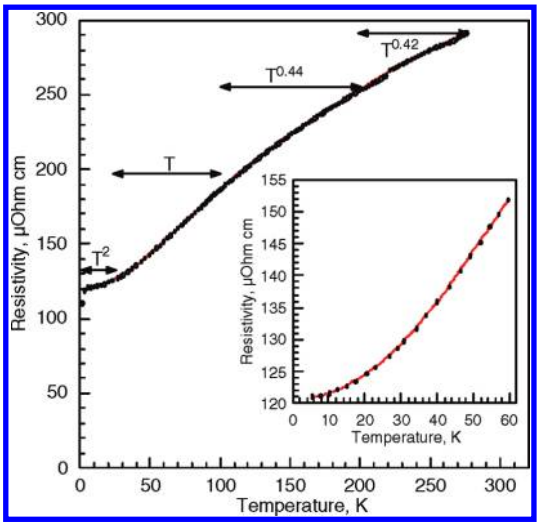

Figure 5. The temperature dependence of the electric resistivity of Y_4FeGa_{12} and its analysis within the framework of spin fluctuation theory. Inset: An enlargement between 0 and 60 K.

Mössbauer Spectra of Y_4FeGa_{12}. Selected iron-57 Mössbauer spectra of Y_4FeGa_{12}, obtained between 4.2 and 295 K, are shown in Figure 6, top left pannel. The solid red lines in Figure 6 are the result of a single line fit (model 1) with the parameters given in Table 4. The single line fit and the absence of any quadrupole splitting is consistent with the cubic symmetry of the iron 2*a* site in the structure of these compounds. The absence of any typical magnetic sextet spectrum below 35 K is somewhat surprising in view of the magnetic properties described above. Only a broadening from 0.28 to 0.41 mm/s of the single absorption line is observed between 40 and 4.2 K. As a consequence, the Mössbauer spectra of Y_4FeGa_{12} obtained below 60 K have, alternatively, been fitted with one symmetric sextet, herein referred to as model 2, with a line width constrained to 0.275 mm/s, the value obtained with model 1 at 60 K; the resulting isomer shifts and hyperfine fields are given in Table 5. It should be noted that the isomer shift is independent of the model used.

The temperature dependence of the hyperfine field in Y_4FeGa_{12} is shown in Figure 7, where the solid line is a parabolic fit between 0 and 30 K with an assumed ordering temperature of 36 K, a fit that follows very well the temperature dependence of the magnetic susceptibility shown in Figure 3a. The 4.2 K hyperfine field of 0.76(1) T is very small, and if the usual conversion factor[20] of 15 T per μ_B for intermetallic compounds is used, this field corresponds to an iron magnetic moment of 0.05 μ_B, a value that is smaller than the zero-field extrapolated value of 0.18 μ_B observed at 3 K in a field of 9 T. However, this conversion factor is valid for intermetallic compounds with localized iron magnetic moments and may not be valid for an itinerant ferromagnet with delocalized magnetic moments. Hence, we believe that the itinerant character of the ferromagnetism in Y_4FeGa_{12} considerably reduces the hyperfine field measured at the iron-57 nucleus. A similar small hyperfine field of 1.64 T has been observed[8] in $NaFe_4Sb_{12}$, which is a weak itinerant ferromagnet with a remanent magnetic moment of 0.28 μ_B/Fe at 1.8 K.

(20) Long, G. J.; Pringle, O. A.; Ezekwenna, P. C.; Mishra, S. R.; Hautot, D.; Grandjean, F. *J. Magn. Magn. Mater.* **1998**, *186*, 10.

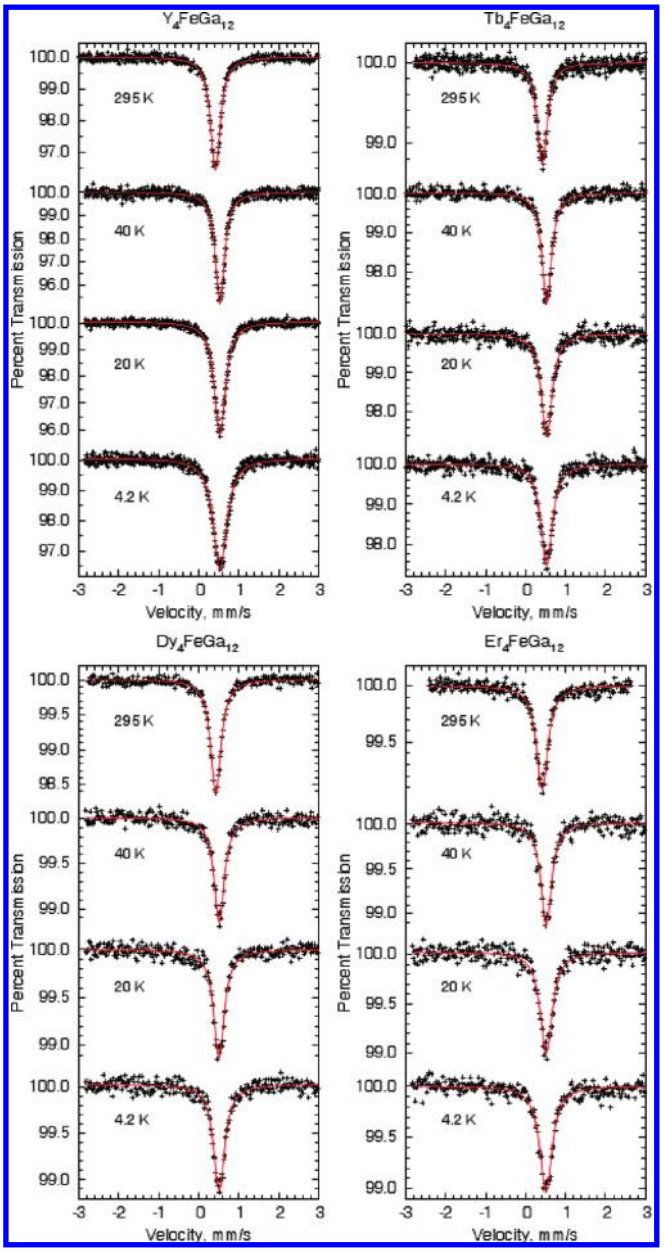

Figure 6. The iron-57 Mössbauer spectra of the Ln_4FeGa_{12} compounds obtained at the indicated temperatures. The solid red lines are the result of a single line fit.

Ln_4FeGa_{12} Physical Properties. For the Ln_4FeGa_{12} compounds, where Ln is Tb, Dy, Ho, and Er, the inverse molar magnetic susceptibility has been fit with the Curie–Weiss law over the temperature range given in Table 6. More specifically, for these fits, $1/\chi = aT + b$, where a is $1/C$, C is the Curie constant, and θ, the Weiss temperature, is $-b/a$. The resulting C and θ values and the corresponding effective magnetic moments, μ_{eff}, obtained from C are given in Table 6.

If the rare earths are assumed to be trivalent cations, a reasonable assumption because the 4f electrons are well-localized and because the magnetic measurements on Y_4FeGa_{12} have shown that there is no localized magnetic moment on the iron, the μ_{eff} in the Ln_4FeGa_{12} compounds, where Ln is Tb, Dy, Ho, and Er, essentially originate in the four rare earths. The corresponding

Table 4. Mössbauer Spectral Parameters for the Model 1 Fits

	isomer shift,[a] mm/s				line width, mm/s			
T, K	Y	Tb	Dy	Er	Y	Tb	Dy	Er
295	0.413(1)	0.415(2)	0.424(2)	0.403(3)	0.298(4)	0.296(7)	0.314(5)	0.36(1)
155	0.500(1)	0.489(3)	0.486(2)	0.484(3)	0.284(2)	0.30(1)	0.314(5)	0.37(1)
85	0.532(2)	0.525(2)	0.511(1)	0.514(3)	0.292(5)	0.299(5)	0.311(1)	0.361(5)
60	0.527(2)	0.529(2)	0.512(3)	0.504(3)	0.275(5)	0.297(5)	0.32(1)	0.35(1)
40	0.529(1)	0.526(2)	0.511(4)	0.504(4)	0.276(2)	0.287(6)	0.31(1)	0.35(1)
30	0.530(3)				0.287(8)			
20	0.526(1)	0.524(3)	0.505(3)	0.504(4)	0.336(3)	0.324(9)	0.32(1)	0.39(1)
10	0.528(1)	0.533(1)			0.390(4)	0.338(2)		
4.2	0.529(2)	0.524(3)	0.509(4)	0.502(4)	0.406(5)	0.342(9)	0.34(1)	0.39(1)

[a] Relative to 295 K α-iron powder.

Table 5. Mössbauer Spectral Parameters for the Model 2 Fits

	isomer shift,[a] mm/s				hyperfine field, T			
T, K	Y	Tb	Dy	Er	Y	Tb	Dy	Er
40	0.529(1)				0.18(4)			
30	0.530(3)				0.28(6)			
20	0.526(1)	0.525(3)	0.505(3)		0.49(1)	0.38(5)	0.33(6)	
10	0.527(1)	0.533(3)			0.71(1)	0.47(3)		
4.2	0.530(2)	0.523(3)	0.509(4)	0.502(4)	0.76(1)	0.48(4)	0.40(6)	0.44(6)

[a] Relative to 295 K α-iron powder.

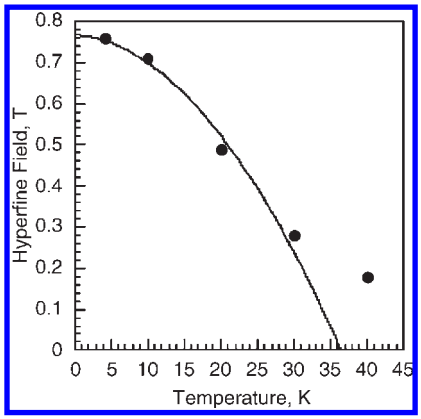

Figure 7. The temperature dependence of the hyperfine field in Y_4FeGa_{12} obtained from a sextet fit with model 2. The solid line corresponds to a parabolic fit between 0 and 30 K and assumed an ordering temperature of 36 K.

expected values of μ_{eff} are given in Table 7. In this approximation, only the lowest-energy, largest-value, rare-earth *J* state is assumed to be populated. The observed μ_{eff}'s are slightly larger than the expected values for Ln = Tb, Dy, and Ho, indicating that the iron contribution to the effective magnetic moments is indeed small but not zero. The observed μ_{eff} for $Er_4Fe_{0.67}Ga_{12}$ is essentially only that arising from the four Er(III). In addition, there is a good linear correlation between the Weiss temperature, θ, and the de Gennes factor, $(g-1)^2J(J+1)$, for the Ln_4FeGa_{12} compounds, a correlation that supports the idea that the molar magnetic susceptibility is dominated by the Ln sublattice.

If a μ_{eff} of 1.265 μ_B is associated with the iron, as determined from the magnetic susceptibility of Y_4FeGa_{12} above 63 K, the expected μ_{eff} for the rare-earth-containing compounds can be considered to arise from the sum of

Table 6. Curie−Weiss Law Derived Magnetic Properties

compound	χ_M^{dia}, emu/mol	temperature range, K	θ, K	*C*, emuK/mol	μ_{eff},[a] μ_B
Y_4FeGa_{12}	−0.000154				
Tb_4FeGa_{12}	−0.000182	100−320	−52.1	47.84	19.56
Dy_4FeGa_{12}	−0.000182	75−320	−29.0(1)	65.26(2)	22.85(1)
Ho_4FeGa_{12}	−0.000182	15−300	−20.8	59.07	21.74
$Er_4Fe_{0.67}Ga_{12}$	−0.000175	15−295	−9.6	45.60	19.10

[a] The effective magnetic moment obtained from the Curie constant, *C*, and uncorrected for the θ value.

Table 7. Expected and Observed Magnetic Properties

Ln(III)	ground state	μ_{eff}, μ_B observed	μ_{eff}, μ_B, calcd per Ln(III)	μ_{eff}, μ_B, calcd per $Ln(III)_4$	μ_{eff}, μ_B, calcd per $Ln(III)_4Fe(Y)$
Tb	$^7F_6$	19.56	9.72	19.44	19.48
Dy	$^6H_{15/2}$	22.85	10.64	21.28	21.32
Ho	$^5I_8$	21.74	10.61	21.22	21.26
Er	$^4I_{15/2}$	19.10	9.58	19.16	19.20

the moments of four Ln(III) ions and one iron moment of 1.265 μ_B and, in this case, $\mu_{eff} = \sqrt{(4\mu_{Ln}^2 + \mu_{Fe}^2)}$. The expected μ_{eff} values obtained with these assumptions are given in the last column of Table 7. The calculated and observed values for Tb are in very good agreement, whereas the observed values for Dy and Ho are larger than the calculated values.

A semilogarithmic plot of the temperature dependence of the molar magnetic susceptibility of the rare-earth-containing Ln_4FeGa_{12} compounds is shown in Figure 8a; the comparable linear plot is shown as Figure S3 in the Supporting Information. All of these rare-earth-containing compounds display an antiferromagnetic-like behavior with a maximum in the susceptibility at 25, 18.5, 9, and 6 K for the Tb, Dy, Ho, and Er compounds, respectively. This antiferromagnetic-like behavior results from the antiferromagnetic ordering of the Ln magnetic moments. However, unlike the molar magnetic susceptibility of a typical antiferromagnetic compound, with the exception of $Er_4Fe_{0.67}Ga_{12}$, the molar susceptibility does not monotonically decrease at temperatures below the maximum but rather remains constant at a value somewhat below that of its maximum. This constant susceptibility at lower temperatures could be the result of spin-canting, but this seems unlikely in an applied field of only 0.1 T. Thus, we believe the susceptibility becomes approximately constant below the maximum because of the

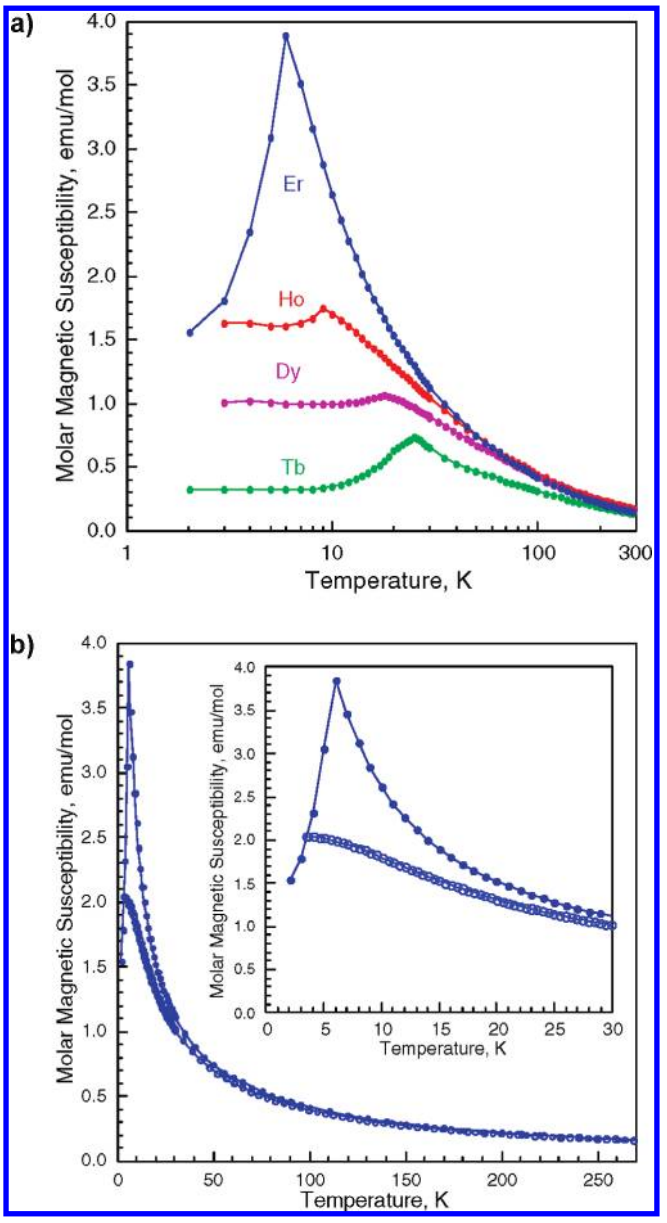

Figure 8. (a) A semi-logarithmic plot of the temperature dependence of the molar magnetic susceptibility of the Ln_4FeGa_{12} compounds measured in a 0.1 T dc applied field. (b) The temperature dependence of the magnetic susceptibility of $Er_4Fe_{0.67}Ga_{12}$ measured at 0.1 T, solid points, and 5 T, larger open points. Inset: The temperature dependence between 3 and 30 K.

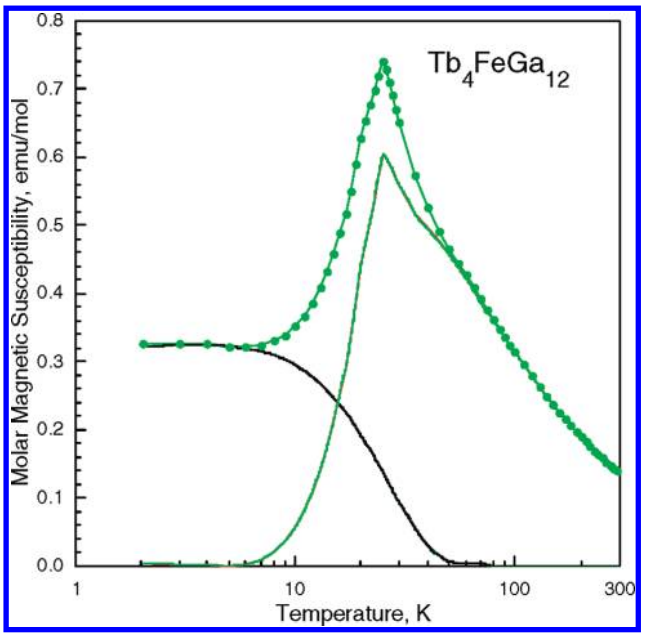

Figure 9. The temperature dependence of the molar magnetic susceptibility of Tb_4FeGa_{12} before, the green points, and after, the green line, subtraction of a 0.45 fraction of the molar magnetic susceptibility of Y_4FeGa_{12}, the black line.

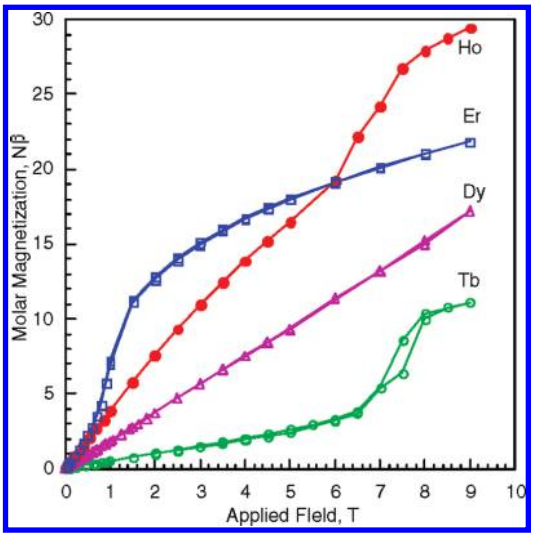

Figure 10. The field dependence of the magnetization of the Ln_4FeGa_{12} compounds measured at 3 K.

temperature-independent Pauli paramagnetic contribution to the susceptibility, as is observed in Y_4FeGa_{12}.

Ideally, one would like to subtract the molar magnetic susceptibility of Y_4FeGa_{12} from those of the rare-earth Ln_4FeGa_{12} compounds in order to obtain the temperature dependence of the contribution of the rare-earth moments to the molar magnetic susceptibility. But, the 2 K magnetic susceptibility observed for Tb_4FeGa_{12} is somewhat smaller than that of Y_4FeGa_{12}, and that of the Ln_4FeGa_{12} compounds, where Ln is Dy, Ho, and Er, is somewhat larger than that of Y_4FeGa_{12}. Hence, below 60 K, a 0.45, 1.53, 2.01, and 0.20 portion of the molar magnetic susceptibility of Y_4FeGa_{12} has been subtracted from the molar susceptibility of the Tb, Dy, Ho, and Er compounds, respectively. The subtraction of the Y_4FeGa_{12} leads to a temperature dependence of the magnetic susceptibility that closely resembles that expected for the antiferromagnetic coupling of the Ln magnetic moments, with Néel temperatures, T_N, of 25, 44, 45, and 8 K, for the Tb, Dy, Ho, and Er compounds, respectively. The result of this subtraction is shown in Figure 9 for Tb_4FeGa_{12}. The various portions used in the subtraction may be a reflection of changes in the band electronic structure upon replacement of Y by Ln.

The temperature dependence of the magnetic susceptibility of $Er_4Fe_{0.67}Ga_{12}$, measured in applied dc fields of 0.1 and 5 T, is shown in Figure 8b. In an applied field of 0.1 T, below a T_N of 8 K, the susceptibility decreases, as expected for an antiferromagnet, whereas in an applied dc field of 5 T, the susceptibility increases as a result of a spin-flop transition.

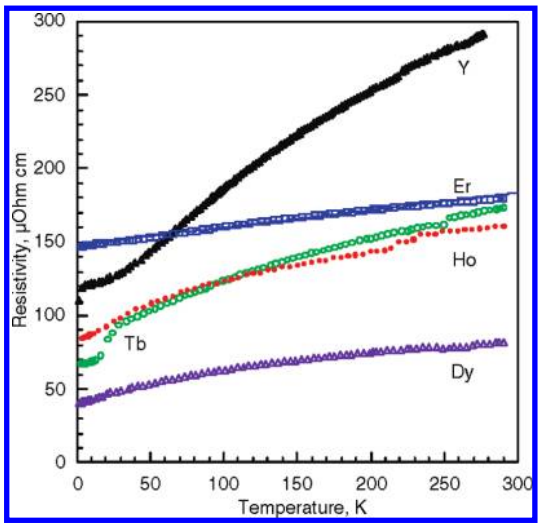

Figure 11. The temperature dependence of the electrical resistivity of the Ln_4FeGa_{12} compounds.

The field dependence of the 3 K magnetization of the rare-earth Ln_4FeGa_{12} compounds is shown in Figure 10. The magnetization of Dy_4FeGa_{12} increases linearly up to 9 T, in a fashion similar to that observed in Dy_4PtGa_{12} and Dy_4PdGa_{12}.[6] Below the critical fields of 6.5, 6, and 1 T, the magnetizations of Tb_4FeGa_{12}, Ho_4FeGa_{12}, and $Er_4Fe_{0.67}Ga_{12}$ increase linearly with the applied field, as would be expected for an antiferromagnetic compound whose magnetic moments are progressively polarized by the applied field. At the critical fields, metamagnetic transitions occur, and in Tb_4FeGa_{12}, the metamagnetic transition is hysteretic between 7 and 8 T. Above 8 T the magnetization is virtually saturated. In Ho_4FeGa_{12}, the magnetization increases noticeably at the metamagnetic transition and more slowly, without saturating, above 7 T. In $Er_4Fe_{0.67}Ga_{12}$, the magnetization increases substantially at the ca. 1 T metamagnetic transition and continues to increase without saturation even at 9 T. We propose that, at the metamagnetic transition, the Ln magnetic moments cant in the applied field, and this canting angle decreases as the field is further increased up to 9 T. Even in a large field of 9 T, the moments are not perfectly aligned in the applied field, and the magnetization is not saturated.

The different field dependence of the magnetization observed for $Er_4Fe_{0.67}Ga_{12}$ likely results from the presence of iron on both the 2*a* and 6*b* sites of the structure, a presence that leads to the occurrence of iron atoms at a distance of 4.238 Å, half the distance between iron atoms in the other Ln_4FeGa_{12} compounds. Further, a binomial distribution of Fe2 neighbors around Fe1 shows that the most likely configurations are one Fe1 atom surrounded by two or three Fe2 atoms. These clusters of iron atoms must be responsible for the different magnetic behavior of $Er_4Fe_{0.67}Ga_{12}$ in the presence of a rather large applied magnetic field.

The temperature dependence of the electrical resistivities of the Ln_4FeGa_{12} compounds is shown in Figure 11, together with that of Y_4FeGa_{12} for comparison. All of the compounds exhibit metallic behavior with increasing resistivity as the temperature increases. The residual resistivity ratios, $\rho(295\ K)/\rho(2\ K)$, are 2.7, 2.0, 1.9, and 1.9, for the Tb, Dy, Ho, and Er compounds, respectively, similar ratios that indicate that the crystal quality of the compounds is similar. Changes in the slope are observed near the ordering temperature, a change that is most obvious in Tb_4FeGa_{12} at ca. 25 K; variations in the slope suggest that the spin-disorder scattering changes at or below the ordering temperature. The larger resistivity of $Er_4Fe_{0.67}Ga_{12}$ probably results from a larger charge scattering by the disordered partially occupied Fe1 and Fe2 sites in the structure.

The magnetoresistance of the Ln_4FeGa_{12} compounds containing Y, Tb, Dy, and Ho is positive at low temperatures but does not exceed 15%. The magnetoresistance of $Er_4Fe_{0.67}Ga_{12}$ is negative with a small value of −0.2% at 9 T.

Mössbauer Spectra of the Ln_4FeGa_{12} Compounds. Selected iron-57 Mössbauer spectra of Tb_4FeGa_{12}, Dy_4FeGa_{12}, and $Er_4Fe_{0.67}Ga_{12}$, obtained between 4.2 and 295 K, are shown in Figure 6. The solid red lines in Figure 6 are the result of a single line fit (model 1), and the resulting isomer shifts, δ, and line widths, Γ, are given in Table 4. Their temperature dependence is shown in Figure 12. The single line fit and the absence of any quadrupole splitting is consistent with the cubic symmetry of the iron 2*a* site in the structure of these compounds.

Interestingly, the observed line width for $Er_4Fe_{0.67}Ga_{12}$ is larger than for the other Ln_4FeGa_{12} compounds. Hence, the Mössbauer spectra of $Er_4Fe_{0.67}Ga_{12}$ do not resolve the two components expected for Fe1 and Fe2 in the 2*a* and 6*b* sites, components that are expected to have similar areas on the basis of the site occupancies by iron. In view of the similarities of the environments of these two sites and their crystallographic equivalence in the $ErGa_3$ structure, this lack of resolution is not surprising. Rather, the presence of two very similar iron components is observed as a line broadening of ca. 50%.

The isomer shifts observed herein are between 0.50 and 0.53 mm/s at 4.2 K and are ca. 0.40 mm/s at 295 K. In the Ln_2Fe_{17},[21−24] $LnFe_{11}Ti$,[25] and $LnCo_{4-x}Fe_xB$[26,27] compounds, the isomer shifts are in the range of zero to 0.2 mm/s at 4.2 K. In contrast, for both iron in a gallium host[28] and iron in Fe_3Ga_4,[29] the isomer shifts are significantly more positive, that is, 0.50 and 0.31 mm/s at 4.2 and 295 K, respectively. In all of the gallium-containing compounds, the iron atoms have gallium near neighbors and share their 3d electrons with these gallium near neighbors. This 3d electron sharing increases the isomer shift as compared to values observed in other intermetallic compounds. The isomer shift decreases from Y to Er in

(21) Long, G. J.; Mishra, S.; Pringle, O. A.; Grandjean, F.; Buschow, K. H. J. *J. Appl. Phys.* **1994**, *75*, 5994.
(22) Hautot, D.; Long, G. J.; Ezekwenna, P. C.; Grandjean, F.; Middleton, D. P.; Buschow, K. H. J. *J. Appl. Phys.* **1998**, *83*, 6736.
(23) Grandjean, F.; Hautot, D.; Long, G. J.; Isnard, O.; Miraglia, S.; Fruchart, D. *J. Appl. Phys.* **1999**, *85*, 4654.
(24) Isnard, O.; Hautot, D.; Long, G. J.; Grandjean, F. *J. Appl. Phys.* **2000**, *88*, 2750.
(25) Piquer, C.; Grandjean, F.; Isnard, O.; Long, G. J. *J. Phys.: Condens. Matter* **2006**, *18*, 205.
(26) Long, G. J.; Hermann, R. P.; Grandjean, F.; Chacon, C.; Isnard, O. *J. Phys.: Condens. Matter* **2006**, *18*, 10765.
(27) Mayot, H.; Isnard, O.; Grandjean, F.; Long, G. J. *J. Appl. Phys.* **2008**, *103*, 94093917 (6 pages).
(28) Shenoy, G. K.; Wagner, F. E.; Kalvius, G. M. In *Mössbauer Isomer Shifts*; Shenoy, G. K., Wagner, F. E., Eds.; North-Holland: Amsterdam, 1978; p 49.
(29) Kobeissi, M. A.; Hutchings, J. A.; Appleyard, P. G.; Thomas, M. F.; Booth, J. G. *J. Phys.: Condens. Matter* **1999**, *11*, 6251.

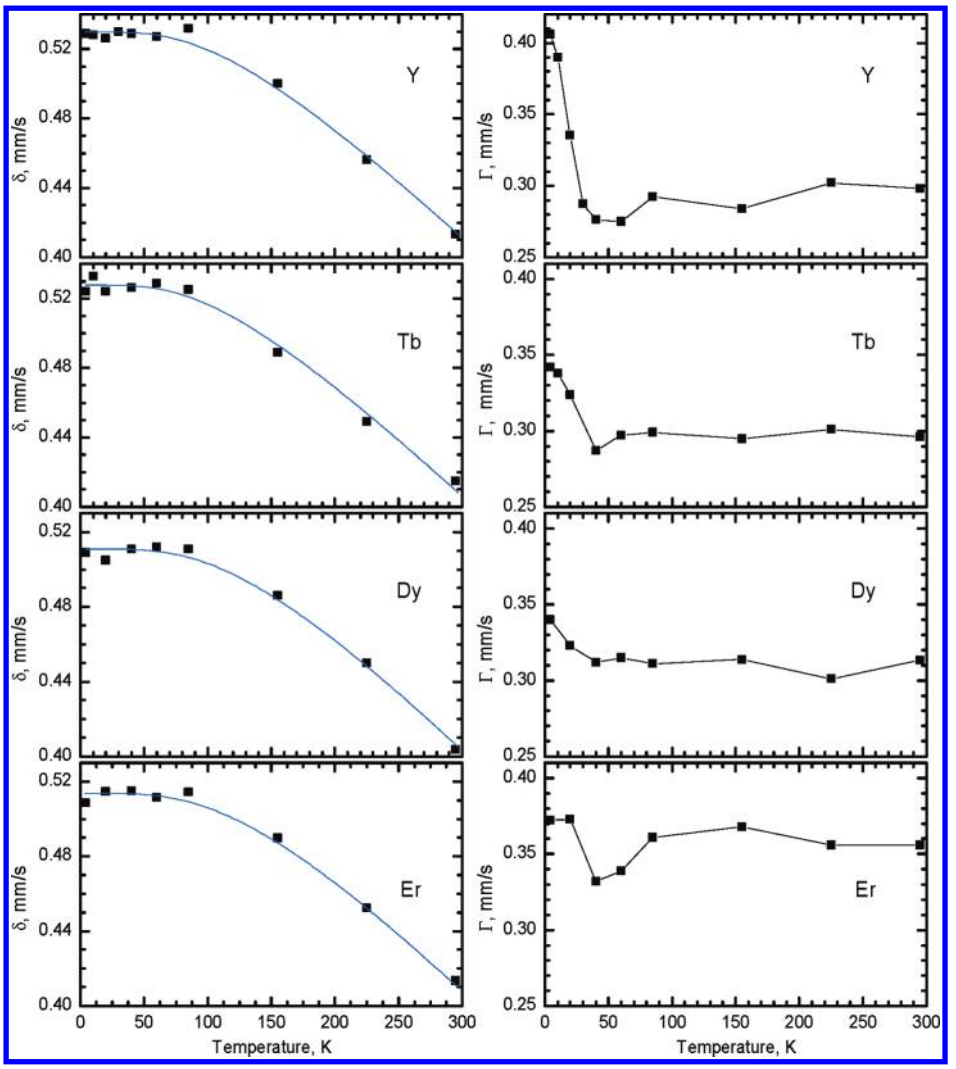

Figure 12. The temperature dependence of the isomer shift, left, and of the line width, right, for the Ln_4FeGa_{12} compounds.

agreement with the lanthanide contraction and the decrease in the unit-cell lattice parameter.

In agreement with the expected second-order Doppler shift, the temperature dependencies of the isomer shifts are well fit with the Debye model for a solid,[28] see the solid lines in Figure 12, left panel. The characteristic Mössbauer temperatures corresponding to these fits are 457(19), 406(26), 610(35), and 499(20) K, for Y_4FeGa_{12}, Tb_4FeGa_{12}, Dy_4FeGa_{12}, and $Er_4Fe_{0.67}Ga_{12}$, respectively. Except for Dy_4FeGa_{12}, these temperatures are only somewhat above the range of 265 to 410 K observed[30,31] for several Ln_2Fe_{17} and $LnCo_{4-x}Fe_xB$ compounds.

Two different temperature dependencies of the line width, Γ, are observed, see Figure 12, right pannel. Below 40 K, the line width observed for Y_4FeGa_{12} increases significantly upon cooling in a fashion similar to the magnetic susceptibility, and this broadening has been interpreted in terms of a small hyperfine field. In contrast, below 40 K, the line width observed for Tb_4FeGa_{12}, Dy_4FeGa_{12}, and $Er_4Fe_{0.67}Ga_{12}$ increases only slightly upon cooling. This different behavior is related to the differences in the magnetic properties of Y_4FeGa_{12} as compared to those of Tb_4FeGa_{12}, Dy_4FeGa_{12}, and $Er_4Fe_{0.67}Ga_{12}$. Y_4FeGa_{12} is a weak itinerant ferromagnet, whereas Tb_4FeGa_{12}, Dy_4FeGa_{12}, and $Er_4Fe_{0.67}Ga_{12}$ are antiferromagnets.

A fit with model 2 of the Mössbauer spectra of the Ln_4FeGa_{12} compounds, where Ln is Tb, Dy, or Er, below their respective Néel temperatures, yields the parameters given in Table 7. These fits give an estimate of the maximum hyperfine field observed at the iron nucleus in these antiferromagnetic compounds. The broadening of the single line Mössbauer spectra observed in the Ln_4FeGa_{12} compounds, when Ln is Tb, Dy, and Er, or the associated extremely small hyperfine fields, may be understood if the eight rare-earth ion near neighbors of the iron are antiferromagnetically coupled and create a zero or nearly zero transferred hyperfine field at the iron nucleus plus any other hyperfine field arising from the spin-polarized itinerant electrons.

The temperature dependence of the logarithm of the spectral absorption area for the Ln_4FeGa_{12} compounds containing Y, Tb, Dy, and Er is shown in Figure 13. The solid lines are the result of a fit with the Debye model for the lattice vibrations. The resulting Debye temperatures are 350(20), 331(19), 239(5), and 345(14) K for Y, Tb, Dy,

(30) Long, G. J.; Isnard, O.; Grandjean, F. *J. Appl. Phys.* **2002**, *91*, 1423.
(31) Mayot, H.; Isnard, O.; Grandjean, F.; Long, G. J. *J. Appl. Phys.*, **2009**, *105*, 113908 (7 pages).

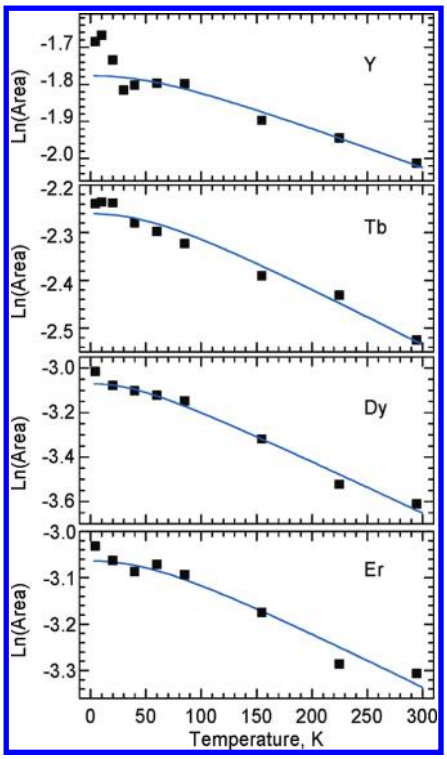

Figure 13. The temperature dependence of the logarithm of the spectral absorption area for the Ln_4FeGa_{12} compounds, with Ln = Y, Tb, Dy, and Er. The blue solid lines are the result of a fit with the Debye model for the lattice vibrations. For Y_4FeGa_{12}, only the areas obtained above 60 K have been used in the fit.

and Er, respectively. These Debye temperatures are related to the mean-square vibrational displacements of the iron nuclei in the lattice, whereas the Mössbauer temperatures obtained from the fit of the temperature dependence of the isomer shifts are related to the mean-square vibrational velocities of the iron nuclei. There is no model-independent relation between these two temperatures, and it is usual to observe larger Mössbauer temperatures than Debye temperatures, because the former probe the high-frequency phonons, whereas the latter probe the low-frequency phonons. In the case of the Ln_4FeGa_{12} compounds, the Mössbauer temperature is approximately 1.5 times the Debye temperature, a factor that is smaller than observed[32,33] in organometallic compounds. The logarithm of the absorption area in Y_4FeGa_{12} shows an increase below 30 K, an increase that is significant and reproducible. This increase must result from a change in the phonon vibrational spectrum at the itinerant ferromagnetic ordering temperature of Y_4FeGa_{12}.

Conclusion

Single crystals of Ln_4FeGa_{12}, where Ln is Y, Tb, Dy, Ho, and Er, have been synthesized, and their structural, magnetic, and electric properties have been investigated between 3 and 320 K. The iron-57 Mössbauer spectra have also been obtained between 4.2 and 295 K. All compounds crystallize in the cubic Y_4PdGa_{12} structure.

Y_4FeGa_{12} is a weak itinerant ferromagnet with an ordering temperature of 36 K and no localized magnetic moment on the iron. In contrast, the Ln_4FeGa_{12} compounds, where Ln is Tb, Dy, Ho, and Er, are both antiferromagnetic with Néel temperatures of 25, 44, 45, and 8 K, as indicated by the temperature dependence of their magnetic susceptibility, and good electric conductors, as indicated by the temperature dependence of their electric resistivity. Hence, there are localized magnetic moments on the Ln(III) cations and most likely some nonzero spin moment on the itinerant electrons. The combination of these two magnetic influences explains the temperature dependence of the magnetic susceptibility, shown in Figure 4a. More specifically, the contribution from the itinerant electrons to the magnetic susceptibility explains the nonzero susceptibility at 0 K. Changes in the spin-up and spin-down populations of the conduction band with the nature of the Ln atom probably result in the various portions of the magnetic susceptibility of Y_4FeGa_{12}, see Figure 9, that have to be subtracted from the magnetic susceptibility of the Ln_4FeGa_{12} compounds, to obtain "typical" antiferromagnetic behavior. A similar variety[7,8,10] of magnetic properties, as a function of the A atoms in AFe_4Sb_{12} filled skutterudites, has been observed.

The iron-57 Mössbauer spectra of Y_4FeGa_{12} and the Ln_4FeGa_{12} compounds, where Ln is Tb, Dy, and Er, obtained above their respective ordering temperature, show single lines, in agreement with the cubic symmetry of the iron 2*a* site. Below 36 K, the single line spectrum of Y_4FeGa_{12} broadens significantly as a result of the small hyperfine field generated by the polarized itinerant electrons at the iron nucleus. The single line spectra of the Ln_4FeGa_{12} compounds, where Ln is Tb, Dy, and Er, broadens only very slightly below their Néel temperatures, as a result of a zero transferred hyperfine field arising from the cancelation of the antiferromagnetically aligned Ln(III) magnetic moments and a very small hyperfine field generated by the polarized itinerant electrons at the iron nucleus. The isomer shifts of the single line spectra are more positive than is observed in many other Ln−Fe intermetallic compounds because of the 3d electron sharing between iron and gallium.

Acknowledgment. J.Y.C. acknowledges NSF (DMR 0756281) and the Alfred P. Sloan Fellowship for partial support of this project. D.P.Y. acknowledges NSF (DMR 0449022). F.G. acknowledges the financial support of the Fonds National de la Recherche Scientifique, grants 9.456595 and 1.5.064.05. The authors would like to thank anonymous reviewer 3 for his very helpful comments that led to a more in-depth understanding of the magnetic properties of the compounds.

Supporting Information Available: Additional Supporting Information is provided in CIF format. This material is available free of charge via the Internet at http://pubs.acs.org.

(32) Reger, D. L.; Elgin, J. D.; Smith, M. D.; Grandjean, F.; Rebbouh, L.; Long, G. J. *Polyhedron* **2006**, *25*, 2616. Reger, D. L.; Gardinier, J. R.; Bakbak, S.; Gemmill, W.; Smith, M. D.; Rebbouh, L.; Grandjean, F.; Shahin, A. M.; Long, G. J. *J. Am. Chem. Soc.* **2005**, *127*, 2303. Reger, D. L.; Gardinier, J. R.; Smith, M. D.; Shahin, A. M.; Long, G. J.; Rebbouh, L.; Grandjean, F. *Inorg. Chem.* **2005**, *44*, 1852. Jiao, J.; Long, G. J.; Rebbouh, L.; Grandjean, F.; Beatty, A. M.; Fehlner, T. P. *J. Am. Chem. Soc.* **2005**, *127*, 17819.

(33) Owen, T.; Grandjean, F.; Long, G. J.; Domasevitch, K. V.; Gerasimchuk, N. *Inorg. Chem.* **2008**, *47*, 8704–8713.